

We are IntechOpen, the world's leading publisher of Open Access books Built by scientists, for scientists

4,800

Open access books available

122,000

International authors and editors

135M

Downloads

Our authors are among the

154

Countries delivered to

TOP 1%

most cited scientists

12.2%

Contributors from top 500 universities



WEB OF SCIENCE™

Selection of our books indexed in the Book Citation Index
in Web of Science™ Core Collection (BKCI)

Interested in publishing with us?
Contact book.department@intechopen.com

Numbers displayed above are based on latest data collected.
For more information visit www.intechopen.com



Single-Photon Frequency Conversion for Quantum Interface

Yuanhua Li and Xianfeng Chen

Abstract

Single-photon frequency conversion for quantum interface plays an important role in quantum communications and networks, which is crucial for the realization of quantum memory, faithful entanglement swapping and quantum teleportation. In this chapter, we will present our recent experiments about single-photon frequency conversion based on quadratic nonlinear processes. Firstly, we demonstrated spectrum compression of broadband single photons at the telecom wavelength to the near-visible window, marking a critical step towards coherent photonic interface. Secondly, we demonstrated the nonlinear interaction between two chirped broadband single-photon-level coherent states, which may be utilized to achieve heralding entanglement at a distance. Finally, we theoretically introduced and experimentally demonstrated single-photon frequency conversion in the telecom band, enabling switching of single photons between dense wavelength-division multiplexing channels. Moreover, quantum entanglement between the photon pair is maintained after the frequency conversion. Our researches have realized three significant quantum interfaces via single-photon frequency conversion, which hold great promise for the development of quantum communications and networks.

Keywords: quantum interface, quantum network, single-photon frequency conversion, periodically poled lithium niobate waveguide, sum frequency generation, cascaded nonlinear process, spectrum compression, spontaneous down-conversion

1. Introduction

In recent years, nonlinear quantum optics has developed rapidly, such as quantum communication [1], quantum computation [2], quantum memory [3], quantum network [4], and so on. In order to realize these quantum applications, coherent quantum interface is a significant quantum device as it is capable of frequency and bandwidth in the telecom band is converted simultaneously. Quantum network is an important platform to study quantum communication, quantum computation, and quantum memory. Quantum network consists of many nodes and the quantum communication channels of the connected nodes, and the quantum communication channels of different connected nodes need to be connected by a quantum interface. Any node in a quantum network has the capability of quantum communication, quantum memory, quantum entanglement swapping, and generation of single photon sources. When the quantum channel of different nodes

performs the conversion of quantum communication and quantum memory, a quantum interface is needed, which can simultaneously realize spectral compression and frequency conversion because the bandwidth and the center frequency of the single photon used in quantum communication and quantum memory are different. When two broadband photons of different nodes' quantum channels are connected by quantum entanglement swapping, the connected quantum interface can efficiently couple the two broadband photons and simultaneously realize the nonlinear frequency conversion of the two broadband photons. The nonlinear up-conversion of two broadband photons in nonlinear crystals can be converted into a high frequency narrowband photon, which provides a basis for implementing different types of quantum interfaces.

Periodically polarized lithium niobate (PPLN) waveguides have higher second-order nonlinear coefficients than other nonlinear crystals. PPLN waveguide not only transmits a wide spectrum but is also easily integrated and processed into PPLN waveguide chips. It also can preserve the quantum properties of photons. The nonlinear effect of PPLN waveguide chip can realize the up-conversion and down-conversion of nonlinear frequencies of different wavelength photons. Therefore, PPLN waveguide chip is ideal for implementing different types of quantum interfaces.

In our work, we utilized PPLN waveguide chip to realize several kinds of different functions of single-photon frequency conversion for coherent quantum interface. First, we have demonstrated the generated coherent quantum interface suitable for quantum communication at 1550 nm and quantum memory in the near-visible window. We exploit a positively chirped single-photon-level laser pulse and a negatively chirped classical laser pulse by sum frequency generation (SFG) process to compress the bandwidth of the positively chirped single-photon-level laser pulse in a PPLN waveguide chip—from 800 to 13.7 GHz—which is approaching the bandwidth regime of some quantum memories. In the same time, one can flexibly convert the 1550-nm telecom-band photons into the near-infrared window [5]. Second, we have experimentally demonstrated the SFG between two broadband single-photon-level coherent states by using a high-efficiency PPLN waveguide chip. The SFG efficiency of 1.06×10^{-7} is realized, which provides potentially feasible quantum applications, such as faithful entanglement swapping without post-selection and nonlinear interaction between single photons with an integrated device at room temperature. What's more, long-distance quantum communication can be achieved by broadband single photons generated in a spontaneous parametric down conversion (SPDC) source [6]. Finally, we have realized the core quantum interface for fiber quantum networks. We report single-photon frequency conversion in a telecommunication band based on cascaded quadratic nonlinearity, i.e., SFG and difference frequency generation (DFG), in a PPLN waveguide. It shows that the frequency of single photons can be precisely converted to a DFG with continuous adjustability in a wide telecommunication band and their quantum characteristics are protected after the single-photon frequency conversion [7].

2. Methodology and result

2.1 Spectral compression of single-photon-level laser pulse

Photons at 1550 nm are critical to all quantum information tasks via an optical-fiber network. Nevertheless, the narrowband photons in the near-visible wavelength regime possess the most efficient quantum memories and an ability of being

easily detected by a silicon avalanche photodiode (APD). Many theoretical schemes have been proposed to achieve the pulse compression or the frequency conversion. For instance, the 1550-nm photons can be converted into the near-infrared window through the nonlinear processes, such as the SFG. As theoretical schemes are diverse, they can be characterized by one common shortage, namely realizing only one operation. Therefore, it is highly expected that an optical technology is capable of simultaneously performing spectrum compression and frequency conversion in the telecom band.

In our experiment, spectral compression of single-photon-level laser pulse is generated by SFG between a positively chirped single-photon-level laser pulse and a negatively chirped classical laser pulse. As known, a laser pulse can be expressed as the frequency-dependent electric field $E(\nu) = U(\nu)e^{i\phi(\nu)}$, where $U(\nu)$ and $\phi(\nu)$ represent the amplitude information and phase information of the laser pulse, respectively. Obviously, we can obtain a chirp result when a transform-limited laser pulse is subject to a quadratic phase $\phi(\nu) \approx A(\nu - \nu_0)^2$, where A is a constant and ν_0 is the center frequency. In terms of $d\phi(\nu)/d\nu = 2\pi t$, one can obtain $d\phi(\nu)/d\nu = 2\pi t = 2A(\nu - \nu_0)$; thus, $\nu = \nu_0 + \pi t/A$ is realized.

The negatively chirped classical laser pulse of frequency with $\nu_{0,P}$ increases linearly in time t_1 , i.e., $\nu_{0,P}(t_1) = \nu_{0,P} + \pi t_1/A$, and the positively chirped single-photon-level pulse frequency with $\nu_{0,Q}$ decreases linearly in time t_2 , $\nu_{0,Q}(t_2) = \nu_{0,Q} - \pi t_2/A$. Here, A is the chirp rate, $\nu_{0,P}$ and $\nu_{0,Q}$ are the center frequency of these two laser pulse sources, and $\Delta t = t_1 - t_2$ is a relative time delay between the negatively chirped classical laser pulse and positively chirped single-photon-level laser pulse. In our work, $\nu_{0,P}$ and $\nu_{0,Q}$ are equal as chirped laser pulse and negatively laser pulse are two replicas of the laser source. When the positively chirped single-photon-level laser pulse and negatively classical laser pulse simultaneously reach the PPLN waveguide chip, a blue-shifted frequency component of negatively classical laser pulse ($\nu_{0,P} + \pi t_1/A$) would match a red-shifted frequency component of positively chirped single-photon-level laser pulse ($\nu_{0,Q} - \pi t_2/A$) with the relative time delay Δt , and all frequency components of these two laser pulses would sum to a new narrow frequency with $\nu_{0,SFG}(\Delta t) = \nu_{0,P} + \nu_{0,Q} + \pi \Delta t/A$. The expected (TH) intensity bandwidth (FWHM) of the SFG photon is given by the following equation [8]:

$$\Delta\nu_{SFG}^{TH} \approx \frac{\ln 4}{A} \sqrt{\frac{1}{\Delta\nu_P^2} + \frac{1}{\Delta\nu_Q^2}}, \quad (1)$$

where $\Delta\nu_P$ and $\Delta\nu_Q$ are the bandwidths (FWHM). The FWHM bandwidth $\Delta\nu$ is limited by group velocity dispersion, and decreases linearly with the length of the PPLN waveguide, i.e., $\Delta\nu = \Delta\hat{\nu}/L$, where $\Delta\hat{\nu} = 4200 \text{ GHz} \cdot \text{cm}$ is the spectral acceptance of the waveguide. When the full FWHM bandwidths of positively chirped single-photon-level laser pulse and negatively chirped classical laser pulse are used in the waveguide, the maximum SFG efficiency is guaranteed.

A schematic of our experimental setup is shown in **Figure 1**. In our experiment, the mode-locked optical-fiber laser pulse source generates 500-fs pulses at 1551.54 nm center wavelength, about 6.4 nm spectral bandwidth (6.4 nm is the FWHM of the spectral intensity distribution), 59.98 MHz repetition rate, and 45.2 MW average power. We split the laser pulse source into two replicas using a 50:50 beam splitter (BS), and then one of the two replicas of laser pulse is sent to a broadband fiber Bragg grating 1 (FBG1); at the same time, the other laser pulse is coupled into the FBG2. The parameters of FBG1 and FBG2 are exactly the same (1547 nm center wavelength, 39 nm FWHM bandwidth, and 5 nm/cm chirp rate).

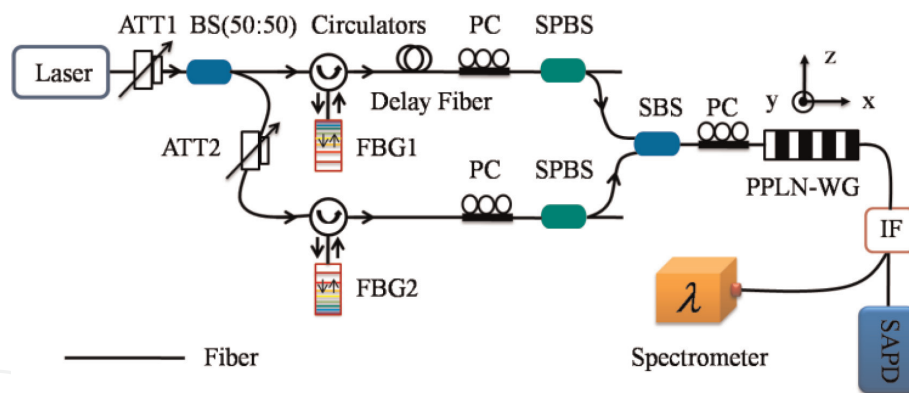


Figure 1.

Experimental set-up. ATT, variable optical attenuator; BS, beam splitter (50:50); Circulators, optical fiber circulators; PC, polarization controller; FBG, fiber Bragg grating; Delay Fiber, optical adjustable delay fiber; SPBS, single mode polarization beam splitter (single mode to polarization maintaining); SBS, single mode beam splitter (single mode to polarization maintaining); PPLN-WG, PPLN waveguide chip; IF, interference filter; SAPD, silicon APD [5].

It is known that FBG can be used for up-chirping and down-chirping, depending on the choice of the side from which the laser pulse is reflected. Thus, the two different chirp laser pulses after FBG1 and FBG2 are the same but with the opposite sign. It means that the positively chirped and negatively laser pulses have an equal and opposite chirp, $\pm A$. A positively chirped laser pulse is generated through FBG1 to introduce a linear chirp by group velocity dispersion. The other laser pulse is negative after a broadband FBG2. A variable optical attenuator (ATT1) is used to create a positively chirped single-photon-level laser pulse, and the other variable optical attenuator (ATT2) is used to control the energy of negatively chirped classical laser pulse for this experiment.

Then, the positively chirped single-photon-level laser pulse and the negatively chirped classical laser pulse are combined by a 1550/1550 nm 50:50 single-mode beam splitter (SBS) and couple into the z-cut PPLN waveguide chip through the optical-fiber pigtail. Two single-mode polarization beam splitters (SPBS (200:1)) and two polarization controllers (PCs) are used for controlling the positively chirped single-photon-level laser pulse and the negatively chirped classical laser pulse to the TM mode; it is known that the PPLN waveguide chip only supports Type-0 ($ee \rightarrow e$) phase matching in our work. A temperature controller (TC) is used for adjusting the PPLN waveguide chip's temperature to keep the QPM of the SFG process. The spectrally narrowed SFG photon pulse can be obtained in the PPLN waveguide chip, after interference filter (IF) with a nominal bandwidth of 20 nm (FWHM) centered around 780 nm (loss is about 1.2 dB), and then coupled into an optical-fiber-coupled spectrometer. Finally, the SFG photons are detected by a SAPD, whose detection efficiency is up to 60% at 775 nm and dark count rate is 26 Hz. In our experiment, a superconducting single photon detector (SSPD) is used to calibrate and monitor the counts of photons of positively chirped single-photon-level laser pulse, whose detection efficiency is up to 10% at 1551 nm and dark count rate is 600 Hz. Using the IF, any residue of the positively or negatively chirped photons have to be filtered out from the SFG photons by a factor of 10^{-18} .

The reverse-proton-exchange PPLN waveguide chip is 52-mm long and QPM to perform the SFG process $1551 \text{ nm} + 1551 \text{ nm} \rightarrow 775.5 \text{ nm}$. It is poled through the quasi-phase-matching period of $19.6 \mu\text{m}$. Moreover, one has a total fiber-to-output-facet throughput of approximately -1.5 dB for the telecom band. The PPLN waveguide chip is antireflection coated to prevent interference fringes and enhance the system efficiency.

We first obtain the spectrum of the positively chirped laser pulse by using an optical-fiber-coupled spectrometer and find a width 800 ± 20 GHz FWHM centered at 1551.54 nm (shown in red). The positively chirped laser pulse is then coupled through an optical fiber and superposed with the negatively chirped classical laser pulse (790 ± 20 GHz, centered at 1551.54 nm) in the PPLN waveguide chip for SFG. The SFG photons, after IF, are sent to a single-mode optical fiber and coupled into the optical-fiber-coupled spectrometer. Here, the FWHM bandwidths of both negatively and positively chirped laser pulses are smaller than the spectral acceptance of the PPLN waveguide chip ($\Delta\nu = \Delta\hat{\nu}/L = 807$ GHz). Thus, the full FWHM bandwidths of positively and negatively chirped laser pulses are used in the PPLN waveguide chip, as expected. As shown in **Figure 2(a)**, we measure significant spectral compression of the positively chirped laser pulse. The initial bandwidth of the positively chirped laser pulse is 800 GHz centered at 1551.54 nm (shown in red). When the quadratic phase is applied and the two laser pulses are up-converted, the bandwidth of laser pulse generated reduces to 33 ± 1 GHz (FWHM) centered at 775.77 nm (shown in black), where the relative time delay $\Delta t = 0$.

Taking the resolution of our spectrometer into account, $\Delta\nu_R = 30 \pm 1$ GHz (FWHM), the actual bandwidth of the SFG photons after deconvolution is $\Delta\nu_{SFG}^{EXP} = \sqrt{\Delta\nu_M^2 - \Delta\nu_R^2} = 13.7 \pm 4.2$ GHz (FWHM). The spectra are given by normalized intensities and, for the up-converted case, correspond to the average of 10 consecutive scans of 15 min acquisition time. This result agrees closely with theory, $\Delta\nu_{SFG}^{TH} = 9.8 \pm 0.7$ GHz (FWHM) from Eq. (1), using the expected chirp parameter $A = (-2.52 \pm 0.01) * 10^8 fs^2$ given by the geometry of our FBG. Therefore, a bandwidth compression ratio of 58:1 is achieved in the positively chirped laser pulse (**Figure 2(b)**).

The center wavelength of the SFG photons can be controlled by adjusting the relative delay Δt between the input pulses at the PPLN waveguide chip. The SFG spectrum of the created laser pulse could be given by a function of the delay time, with the fitted center wavelengths shown in **Figure 3**. The experimental results show that the wavelength depends linearly on the delay time, as expected. The linear fit gives a slope of -0.0247 ± 0.001 nm/ps. In terms of the slope data, we measure the negatively chirp parameter of $A = (-2.55 \pm 0.01) * 10^8 fs^2$, in good agreement with the chirp parameter $A = (-2.52 \pm 0.01) * 10^8 fs^2$ of the FBG1. It is also shown that the bandwidth compression ratio independent of the optical relative delay Δt , which agrees closely with the theoretical result from the above Eq. (1).

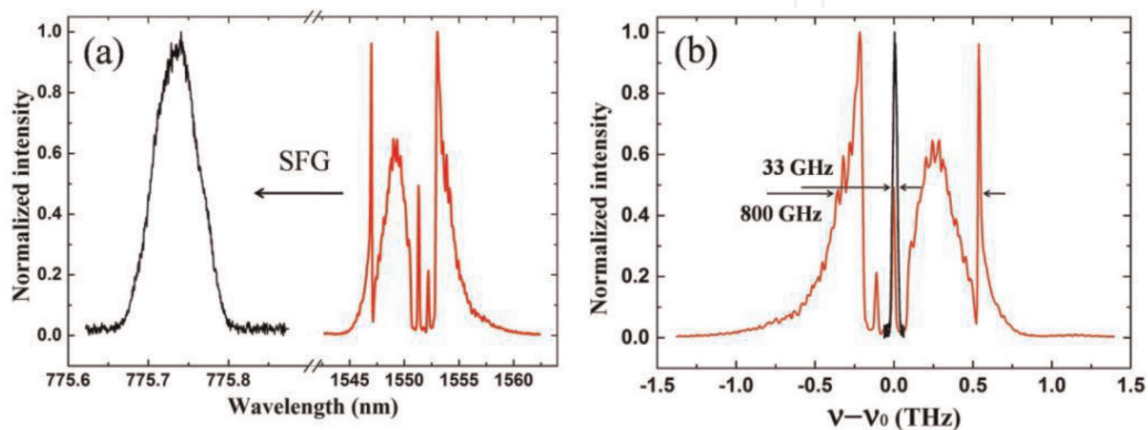


Figure 2. The positively chirped pulse spectrum and up-converted laser pulse spectrum (a) and relative frequency (b) [5].

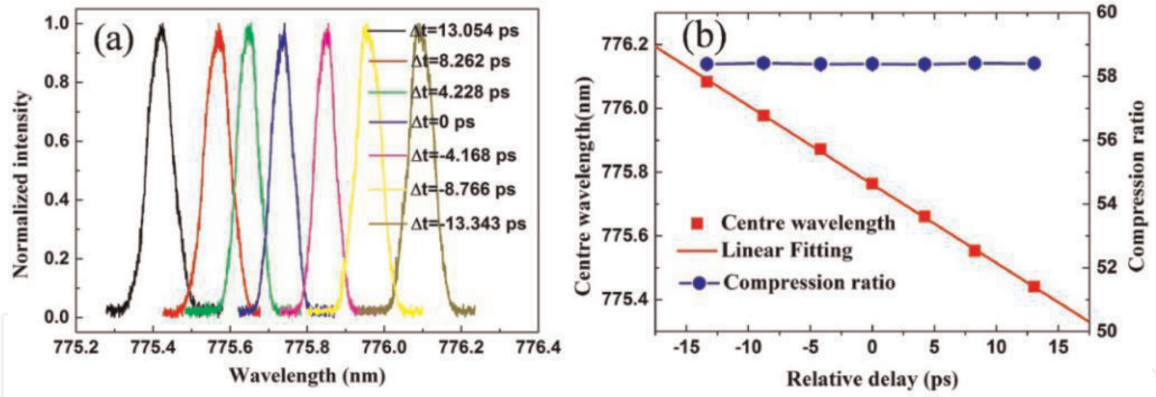


Figure 3.

The SFG spectrum of the created laser pulse (a), central wavelength and compression ratio of the output pulses versus the optical relative delay (b). Error bars are smaller than the data points [5].

In our experiment, it is verified that any SFG photons detected by the SAPD is the result of the SFG process, and not a SHG of the positively or negatively chirped photons. Moreover, any residue of photons the positively or negatively chirped laser pulse has to be filtered out from SFG photons by a factor of 10^{-18} . Once the number of positively chirped laser pulse is controlled to single-photon level, the detected SHG counts from the positively chirped laser pulse drop to its dark counts (3.5 Hz). When the input power of the negatively chirped laser pulse is less than 0.6 nW, the SHG photons are also equal to the dark counts. The efficiency of SFG is then given by $\eta_{SFG} = P_{SFG}/\beta N$, where P_{SFG} is the number of SFG photons per second, β is the repetition rate of seed laser, and N is average of photons per second of positively chirped laser pulse.

As shown in **Figure 4**, the power of the negatively chirped laser pulse is keeping at 0.6 nW. The SFG photons and SFG efficiencies are measured. The average of photons per second ($N_1 = 0.933$ and $N_2 = 0.302$) of positively chirped laser pulse can be obtained with the ATT2. By adjusting the relative delay Δt , SFG photons and SFG efficiencies of different situations are measured (like **Figure 3(b)**). At the same time, it is found that the overall conversion efficiency of SFG varies with the relative delay Δt . When the relative time delay $\Delta t = 0$, the maximum SFG efficiency is 7.82×10^{-6} with the average of photons of positively chirped laser pulse (0.933), where the dark counts (3.5 Hz) are subtracted. Here, the total losses have

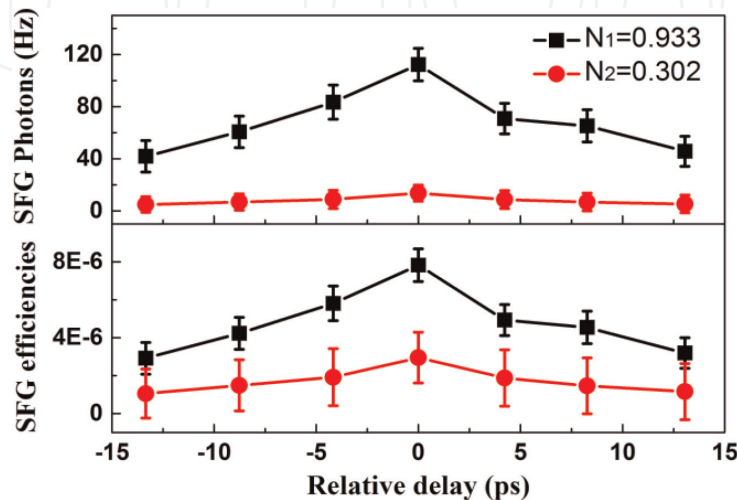


Figure 4.

SFG photons (top) and SFG efficiencies (bottom). The abscissa is a variable optical relative delay between the negatively and positively chirped laser pulses at the PPLN waveguide chip [5].

been considered, such as the coupling loss of 0.7 dB, reflection loss of 1.2 dB, total fiber-to-output-facet loss of 1.5 dB, and detection efficiency of 60% (see **Figure 4**).

The lower SFG signal for single photons required longer times than for the intense photons states. Thus, all the data are measured within a day to reduce the effects of drift. The results show that the SFG efficiency increases with increasing the average of photons of the positively chirped pulse (see **Figure 4**).

It is found that the SFG efficiency decreases with reducing the photons of negatively chirped laser pulse, and the efficiency of SFG also increases with increasing input power of the positively and negatively chirped laser pulse. Next, we obtain the efficiency of SFG in two ways: one, by controlling the photons of the negatively chirped laser pulse with the ATT1 and ATT2; the other by increasing the power of positively and negatively chirped laser pulse with the ATT1 and ATT2. **Figure 5** depicts the results of these two measurements. The SFG efficiencies, SFG photons, the power of produced harmonics, and error bars of them are accounted, where the dark counts (3.5 Hz) are subtracted.

As shown in **Figure 5(a)**, when the negatively chirped laser pulse (10 photons per pulse) and the positively chirped single-photon-level laser pulse (0.933 photons per pulse) are simultaneously sent to the PPLN waveguide chip, the maximum SFG efficiency of 4.58×10^{-7} is obtained, where the relative time delay $\Delta t = 0$. In **Figure 5(b)**, we use the ATT1 and ATT2 to keep the input power of positively and negatively chirped laser pulse at 203.1 and 202.8 μW , respectively. The power of produced harmonics $E_i (i = 0, 1, 2)$ can be measured, where E_0 is the total power of SFG and SHG of the positively and negatively chirped laser pulse, E_1 is the power of SHG of the positively chirped laser pulse, and E_2 is the power of SHG of the negatively chirped laser pulse. When the relative time delay $\Delta t = 0$, the power of SHG generated is $E_0 = 21.62 \mu\text{W}$, which is obtained from SHG of the positively chirped laser pulse ($E_1 = 0.28 \mu\text{W}$), SHG of the negatively chirped laser pulse ($E_2 = 0.01 \mu\text{W}$), and SFG photons ($E_{SFG} = E_0 - E_1 - E_2 = 21.33 \mu\text{W}$). In the case, the maximum SFG efficiency of 20% is obtained, where the relative time delay $\Delta t = 0$. Here, the total losses have been taken into account. We also find that the rate of SFG photons generated is 73 times of the rate of SHG photons generated of these two independent laser pulses.

In our scheme, although both the negatively and positively chirped laser pulses are at the same center wavelength, the power of SHG from each is kept below the power of SFG (see **Figure 5(b)**). At the same time, the SHG photons from the two independent laser pulses are also lower than the SFG photons when the bandwidth of positively chirped single-photon-level laser pulse is compressed

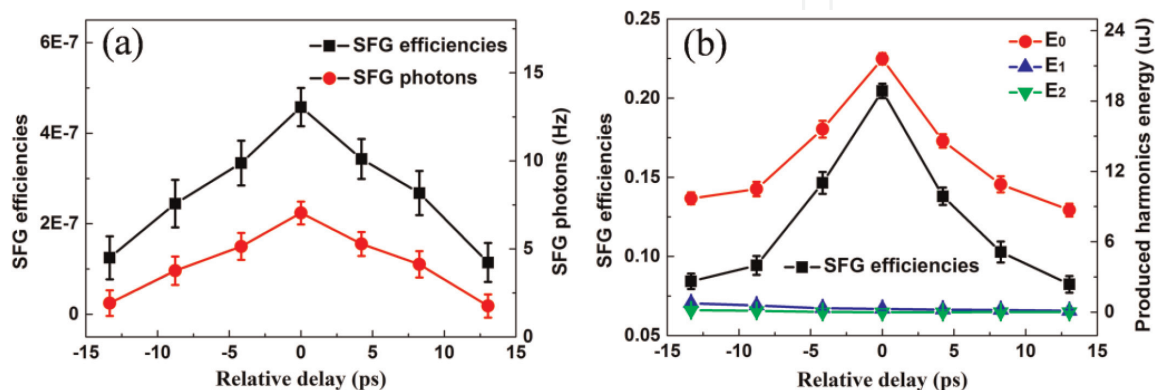
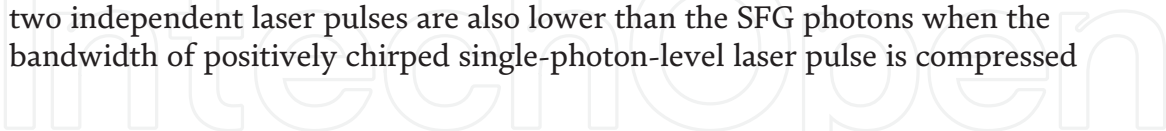


Figure 5. SFG photons and SFG efficiencies (a), SFG efficiencies and the energy of generated SHG photons (b). The abscissa is a variable optical relative time delay between the negatively and positively chirped laser pulses at the PPLN waveguide chip [5].

(see **Figures 4** and **5(a)**). We can also confirm that by controlling the power of the negatively chirped laser pulse, considering a positively chirped single-photon-level laser pulse (0.933 photons per pulse). **Figure 6** depicts the results of experimental and theoretical SFG and SHG.

Once the input power of the negatively chirped laser pulse is more than 0.6 nW, the up-converted photons generated consists of SHG photons of the negatively chirped laser pulse, and SFG photons of the negatively chirped laser pulse and the positively chirped single-photon-level laser pulse. In our experiment, up-converted photons cannot be filtered out separately; thus, the SFG photons P_{SFG} cannot be measured. Here, we first send the negatively chirped laser pulse to the PPLN waveguide chip alone, and the SHG photons P_1 of the negatively chirped laser pulse can be measured. If we simultaneously couple the negatively chirped laser pulse and positively chirped single-photon-level laser pulse together into the PPLN waveguide chip, the photons P_0 of SFG and SHG can be obtained. The SFG photons generated are obtained with the equation $P_{SFG} = P_0 - P_1$. When the relative time delay $\Delta t = 0$, the SHG and SFG photons of different situations are obtained by controlling the power of the negatively chirped laser pulse (see **Figure 6(a)**). When the power of negatively chirped laser pulse is less than 4.8 nW, we find that SHG photons generated are lower than the SFG photons generated. When $P_{SFG} = P_1$, the SFG efficiency of 3.12×10^{-5} is obtained. The measured results show that the number of SHG photons will be more than the number of SFG photons when the power of negatively chirped laser pulse is more than 4.8 nW.

Next, we carry out the theoretical analysis for SHG and SFG photons. As shown in **Figure 6(b)**, the spectrum of the negatively chirped laser pulse is measured. It is found that the intensity of the negatively chirped laser pulse at 1551.54 nm is very close to zero. When the negatively chirped laser pulse is sent to the PPLN waveguide alone, the number of SHG photons generated is very low. Here, we assume that the power of the negatively chirped laser pulse which can be converted into SHG photons is E_{N_2} (black area), thus, the SHG photons $P_1 \propto |E_{N_2}|^2$. However, when the negatively and positively chirped laser pulses are simultaneously couple together into the PPLN waveguide chip, photons in all spectrum of the negatively chirped laser pulse can be used to produce the SFG photons. The full power of the negatively chirped laser pulse is E_{N_1} , as shown in **Figure 6(b)**. Thus, the SFG photons $P_{SFG} \propto E_{N_1} E_S$, where E_S is the power of the positively chirped single-photon-level laser pulse. When $P_{SFG}/P_1 \geq 1$, the number of SFG photons generated is more than the number of SHG photons. In the case, we obtain

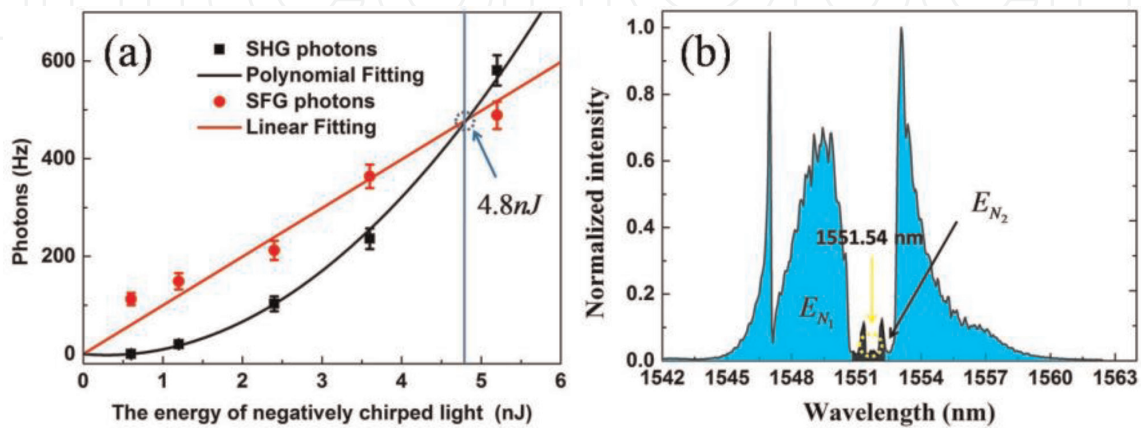


Figure 6.

SHG photons and SFG photons (a), the negatively chirped laser pulse spectrum (b). The dark counts (3.5 Hz) are subtracted, and the error bars are accounted [5].

$$\frac{E_{N_1} E_S}{|E_{N_2}|^2} \geq 1. \quad (2)$$

In terms of $E_{N_1} = qE_{N_2}$, one can obtain $E_{N_1} \leq q^2 E_S$, where q is proportional coefficient. In our experiment, one has $E_S = 7.3 \times 10^{-3}$ nJ and $q = 26.8$; thus, $E_{N_1} \leq 5.2$ nJ is realized. This result agrees closely with experiment, as shown in **Figure 6(a)**.

In order to reduce the number of SHG photons to the dark counts (3.5 Hz), the power of the negatively chirped laser pulse must be very low. Thus, the SFG efficiency is limited. The way to improve SFG efficiency is to filter out the photons of wavelengths centered at 1551.54 nm of the negatively chirped laser pulse.

Furthermore, our results may provide potential application in standard decoy-state quantum key distribution. By considering a fiber attenuation of 0.2 dB/km, the coupling loss of 0.7 dB, the dark counts of 3.5 Hz, total fiber-to-output-facet loss of 1.5 dB, reflection loss of 1.2 dB, detection efficiency of 60%, and laser pulse with a 59.98 MHz repetition rate, the SFG efficiency of 7.82×10^{-6} will achieve a rate of about 8 bits/h on a distance of 20 km.

2.2 Nonlinear interaction between broadband single-photon-level coherent states

It has been demonstrated that parametric interactions hold numerous advanced applications in quantum communication, but strong optical fields are usually used to preserve quantum property [9]. Nonlinear interactions between single photons have been experimentally measured, such as spontaneous down-conversion [10] and cross-phase modulation [11]. Here, we take the next step and report, a SFG between two broadband single-photon-level coherent states. In our experiment, the SFG efficiency of 1.06×10^{-7} is realized, which provides potentially feasible quantum applications, such as faithful entanglement swapping without post-selection and nonlinear interaction between single photons with an integrated device at room temperature. What's more, long-distance quantum communication can be achieved by broadband single photons generated in a spontaneous parametric down conversion (SPDC) source.

In our experiment, a mode-locked optical fiber laser generates 500-fs pulses at 1551 nm with a repetition of 59.98 MHz and is used to generate the two chirped broadband single-photon-level coherent states after FBG1 and FBG2. These two chirped broadband coherent states are combined via a 50:50 SBS and sent to a PPLN waveguide chip. The PPLN waveguide chip length is 52 mm, and its total losses are 2.2 dB including a coupling loss of 0.7 dB and a total fiber-to-output-facet loss of 1.5 dB. The unconverted photons are deterministically separated from the SFG photons after IF, and the SFG photons are coupled into a silicon APD.

A schematic of the experimental setup is shown in **Figure 7**. The mode-locked optical fiber laser can generate two copies of the pulses with equal energy with a 50:50 BS. These two copies of the pulses are used to produce two broadband single-photon-level coherent states with ATT1 and ATT2. One of the two copies of the laser pulses is couple into the FBG1, and the other laser pulse is coupled into the FBG2. Thus, the spectrums of two copies of the photons after FBG1 and FBG2 are the same but with the opposite sign. In our experiment, the positively chirped single-photon-level coherent state is generated with the FBG2, and the other single-photon-level coherent state is the negatively chirped coherent state after the FBG1.

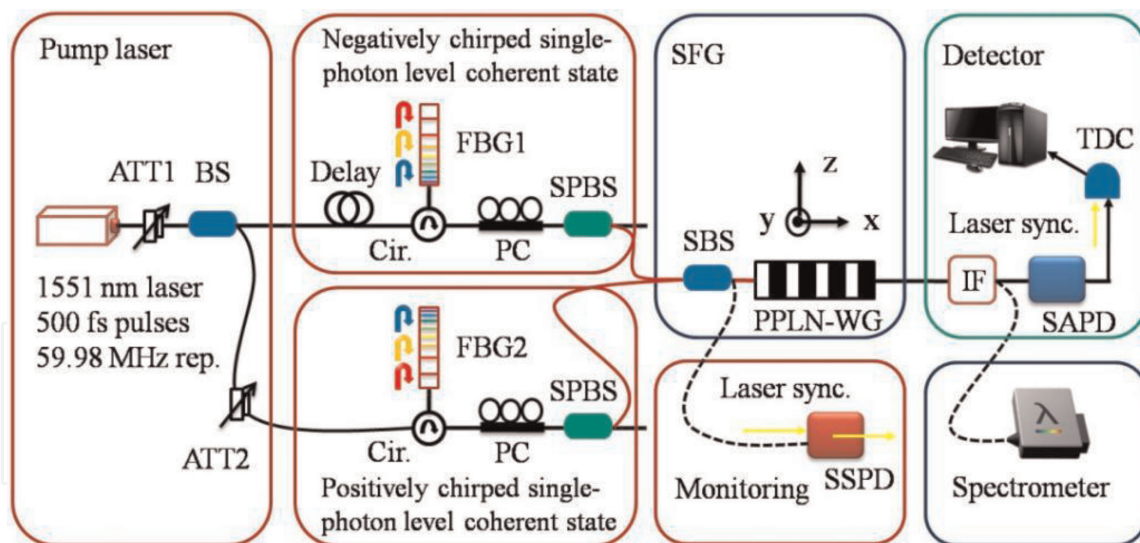


Figure 7.

Experimental set-up. ATT, variable optical attenuator; BS, beam splitter (50:50); Circulators, optical fiber circulators; PC, polarization controller; FBG, fiber Bragg grating; Delay Fiber, optical adjustable delay fiber; SPBS, single mode polarization beam splitter (single mode to polarization maintaining); SBS, single mode beam splitter (single mode to polarization maintaining); PPLN-WG, PPLN waveguide chip; IF, interference filter; SAPD, silicon APD [6].

The FBG can be used to produce the up-chirping and down-chirping, depending on the choice of the side from which the laser pulse is reflected. As the two copies of the laser pulses are from the same seed laser, they have the same initially center frequency ω_0 . When two copies of the laser pulses with instantaneous frequencies described as $\omega_1(t) = \omega_0 + At$ and $\omega_2(t) = \omega_0 - At$ (where A is the linear chirp parameter) undergo SFG, the frequency of the laser pulse generated is constant ($\omega_1(t) + \omega_2(t) = 2\omega_0$); thus, the high frequency long narrowband laser pulse can be realized.

Subsequently, the positively and negatively chirped coherent states are sent to the PPLN waveguide chip by the fiber pigtail. The PPLN waveguide chip is a reverse-proton-exchange waveguide that is QPM to perform the SFG process $1551 \text{ nm} + 1551 \text{ nm} \rightarrow 775.5 \text{ nm}$. The PPLN waveguide chip has a QPM period of $19.6 \mu\text{m}$. Two SPBS (200:1) and two PCs are used for controlling the positively and negatively chirped single-photon-level coherent states to the TM mode. A SSPD is used to calibrate and monitor the counts of the positively and negatively chirped single-photon-level photons, whose detection efficiency is up to 10% at 1551 nm and dark count rate of 600 Hz. A stable TC is used to keep at 27° to maintain the QPM condition of the SFG process. The long narrowed SFG photons of higher frequency are generated after the IF, with 20 nm FWHM bandwidth and 780 nm center wavelength (about 1.2 dB loss). Finally, the SFG photons are detected with a SAPD. The SFG photons and the laser clock signal are recorded using a TDC.

We first measure the spectrums of the negatively chirped laser pulse (800 ± 20 GHz spectral FWHM bandwidth, and 1551.56 nm center wavelength) and the positively chirped laser pulse (790 ± 20 GHz FWHM, and 1551.56 nm center wavelength) by using a spectrometer, which are shown in **Figure 8(a)**. The pump light (the negatively chirped laser pulse) and the signal light (the positively chirped laser pulse) are simultaneously sent to the PPLN waveguide chip. By using an IF, the generated SFG photons are sent into the spectrometer.

In our experiment, when the classical pump and signal laser pulses are coupled into the PPLN waveguide chip, the up-converted photons consist of SHG of pump light, SHG of signal light, and SFG of pump light and signal light. In our experiment, up-converted photons cannot be filtered out separately; thus, the SFG

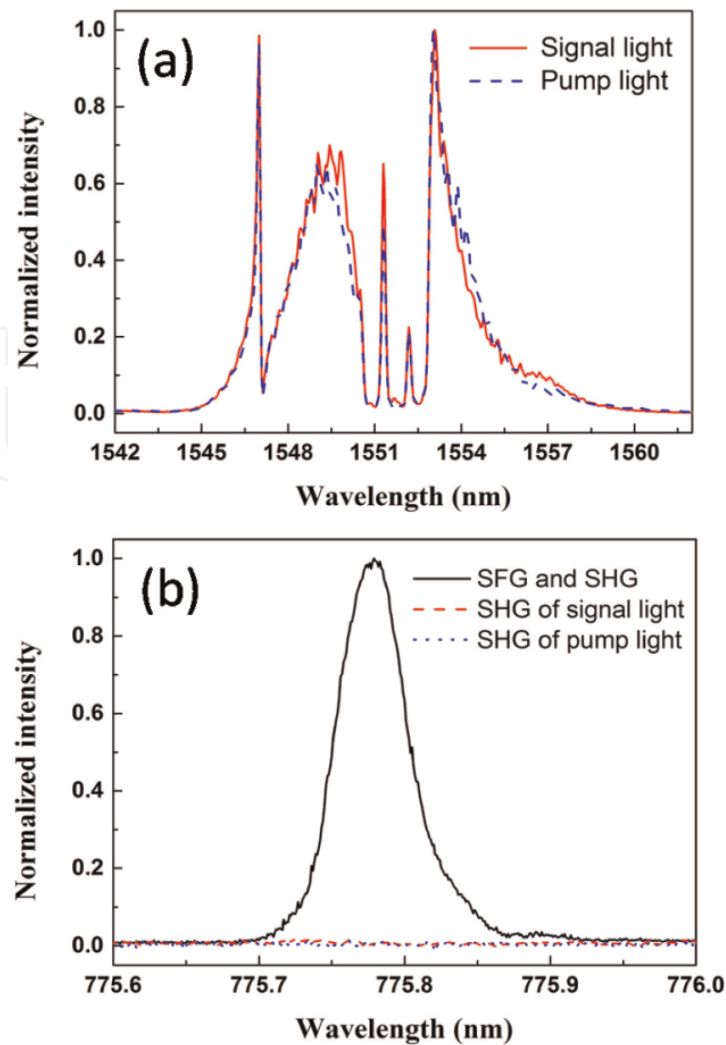


Figure 8. Pump and signal light spectrums (a), and the spectrums of up-converted light (SFG and SHG), SHG of signal light, SHG of pump light (b) [6].

photons N_{SFG} cannot be measured. First, the pump light is sent to the PPLN waveguide chip alone, and the number of SHG photons N_1 can be obtained. Similarly, the number of SHG photons N_2 of signal light is obtained when only the signal light is sent to the PPLN waveguide chip alone. When we simultaneously couple the pump and signal laser pulses together into the PPLN waveguide chip, we can obtain the number of photons N_0 of SFG and SHG. Therefore, the number of SFG photons is obtained with the equation $N_{SFG} = N_0 - N_1 - N_2$. For the SFG photons to be measured distinctly, any residue of pump and signal light has to be filtered out from up-conversion photons in this work. Here, the efficiency of SFG is given by $\eta_{SFG} = N_{SFG}/N_A$, where N_A is the number of photons per second of the signal light.

For instance, the input power of the signal and pump light is keeping at 200.2 and 200.4 μW , respectively. When they are simultaneously sent to the PPLN waveguide chip, the FWHM bandwidth and power of the created up-conversion light can be measured. If pump light (or signal light) is sent to the PPLN waveguide chip alone, the bandwidth and power of SHG of pump light (or signal light) can be obtained. When the PPLN waveguide chip's temperature is kept at 27°, as shown in **Figure 8(b)**, the FWHM bandwidth of the created up-conversion light is about 0.07 nm, centered at 775.78 nm. In this case, the power of up-conversion light is 20.9 μW (involving the SFG and SHG), which is obtained from SHG of signal light (0.25 μW), SHG of pump light (0.01 μW), and SFG of pump light and signal light (20.54 μW). The maximum SFG efficiency of 5% is obtained, which is used for

estimating the efficiency of SFG between two single-photon-level states in our work. As shown in **Figure 9**, the efficiency of SFG depends on the PPLN waveguide chip's temperature. Correcting for all of these losses, the intrinsic device maximum SFG efficiency of 20% is obtained, as expected.

When the number of photons per pulse of pump light and signal light is attenuated to 5.13 and 5.64, respectively, the detected count of SHG of signal light (or pump light) drop to 3.8 Hz (dark count). It can be shown that any photons detected by the SPAD are the SFG photons when the signal and pump light are attenuated to single-photon-per-pulse simultaneously. Therefore, photons of SHG of pump light and signal light are not considered in our scheme.

In our experiment, the number of photons per pulse (equal for pump and signal) are obtained with ATT1 and ATT2, as they can be detected and calibrated by the SSPD. According to our experimental results, the SFG efficiency and SFG photons are shown in **Figure 10**. Here, dark counts of 3.8 Hz and the total losses of about 5.6 dB have been taken into account.

The overall conversion efficiency of SFG is given by $\eta'_{SFG} = \xi(\lambda)hc\Delta\nu L^2/\lambda t b p$, where $\xi(\lambda)$ is the measured up-conversion efficiency of the PPLN waveguide chip, λ is the center wavelength of pump light, $t b p$ is the time-bandwidth product, $\Delta\nu$ is the bandwidth of pump light, and L is the length of the PPLN waveguide chip. Consider that $\xi(\lambda) = 5\%/(W \cdot cm^2)$ and $t b p = 0.4$ in our experiment, thus the expected SFG efficiency is $\eta'_{SFG} \approx 1 \times 10^{-7}$. We measure the efficiency of $\eta_{SFG} = (1.06 \pm 0.23) \times 10^{-7}$. It is shown that the SFG efficiency is high enough to provide efficient, yet simpler solutions to linear optics based protocols for the heralded creation of maximally entangled pairs or for the implementation of device-independent quantum key distribution.

For SFG between two single photons, our efficiency of SFG is about eight times of the efficiency of SFG given by Sangouard et al. [12]. When the single-photon-level pump and signal light are not chirped in our experiment, the SFG photons are zero. This is because the intensity of pump light (or signal light) at 1551.56 nm is very low (see **Figure 8(a)**). However, when the negatively and positively chirped pulses are simultaneously coupled into the PPLN waveguide chip, photons in all spectrums of the negatively and positively chirped light are used to create the SFG photons. Therefore, we can improve the efficiency of SFG between single photons by using the chirped technology.

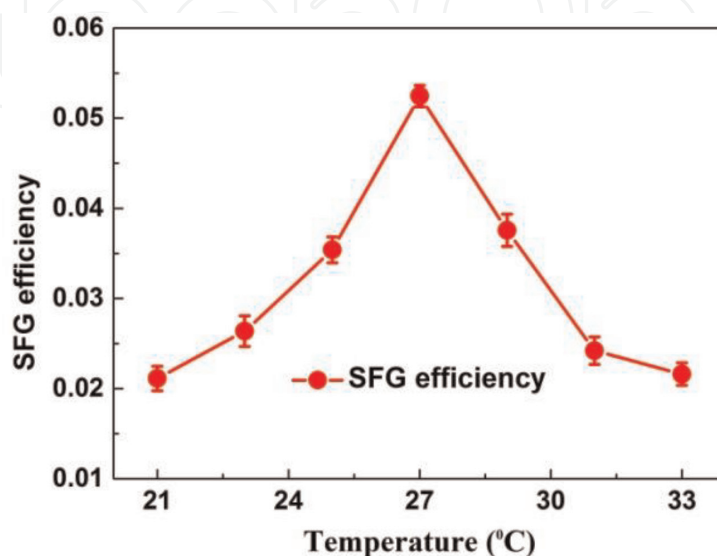


Figure 9. SFG efficiency. The efficiency of SFG can be controlled by keeping the PPLN-WG chip's temperature [6].

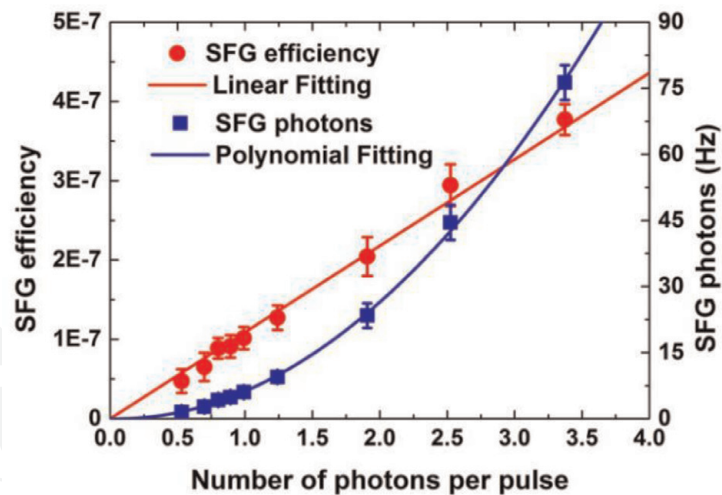


Figure 10.
SFG efficiency and SFG photons [6].

2.3 Single-photon frequency conversion via cascaded quadratic nonlinear processes

In quantum networks, many nodes are needed, which are used to perform quantum information memory/processing tasks. Each node has the ability to generate quantum states and perform quantum Bell-state measurements. All nodes are connected by using optical fibers. Frequency conversion has important applications in fiber quantum networks, and frequency converters are set to light. At the intermediate node of the fiber quantum network, the information transmission mode of the corresponding wavelength is obtained, and the specific wavelength signal carrying the information is transferred to the other wavelength. The development of this technology has greatly improved the transmission capacity of the optical network and the flexibility of the entire network.

In addition to the frequency conversion between the communication band and the visible band, single-photon frequency conversion between communication bands, like classical fiber networks, has important applications in large-scale quantum networks, as well as between independent sources of different users. Quantum cryptic transmission or quantum key distribution also requires different wavelengths to be converted to coincidence before interference. Therefore, the single photon frequency conversion interface between communication bands is critical in quantum communication.

However, there are not many experiments to achieve single-photon frequency conversion in the communication band. There are only two known solutions and each of these experimental solutions has imperfections. The first solution is to achieve high-precision frequency conversion by optical single sideband modulator (OSSB). This method can eliminate the frequency distinguishability between different single photons, but the frequency conversion range that this scheme can achieve covers only dozens. Gigahertz does not meet the requirements of communication networks. The second scheme is consistent with the four-wave mixing principle of the classical light in the previous section. The third-order nonlinearity of the optical fiber is used to realize the frequency conversion of the communication band, but we know that the third-order nonlinear coefficient is much smaller than 2. The order nonlinear coefficient, thus one must use 750 m long fiber, which is very unfavorable for device integration.

In order to make up for the shortcomings of the above two schemes, we use the high second-order nonlinear coefficients of the PPLN waveguide and the wide-band

type-0 quasi-phase matching to realize the single-photon frequency conversion based on the cascaded second-order nonlinear process. In the experiment, we realized the precise frequency conversion between DWDM channels through the cascading process of SFG + DFG. At the same time, we also proved that the quantum characteristics of single photons remain in this process. Our experiment is very suitable for the construction of quantum networks.

The nonlinear process of frequency conversion of a single photon can be described by the following effective Hamiltonian [13]:

$$\hat{H} = i\hbar(\chi_1 E_{P1} \hat{\alpha}_s \hat{\alpha}_m^\dagger + \chi_2 E_{P2} \hat{\alpha}_m \hat{\alpha}_t^\dagger - \text{H.c.}), \quad (3)$$

where $\hat{\alpha}_i$ is the annihilation operator for the wave at frequency ω_i , ($i = s; m; t$ is signal, mediate, and target photons, respectively). $\chi_{1,2}$ are coupling constants that are proportional to the second-order susceptibility $\chi^{(2)}$ of the PPLN waveguide chip, E_{P1} and E_{P2} are the electric field amplitudes of pump lasers, and H.c. is a Hermitian conjugate. The conversion efficiency η_c can be obtained by using the Heisenberg equation of motion, which is given by the following equation:

$$\eta_c(L) = \frac{\eta_1 \eta_2 P_{P1} P_{P2} |\cos[2(\varphi_1 - \varphi_2)]|}{(\eta_1 P_{P1} + \eta_2 P_{P2})} \times \left\{ 1 - \cos[\eta_1 P_{P1} + \eta_2 P_{P2}]^{(1/2)} L \right\}^2, \quad (4)$$

where φ_1 and φ_2 are the phases of the two pumps, respectively. η_1 and η_2 are the efficiencies of the normalized power, and $\eta_1 \approx \eta_2 = 1.1/W \text{ cm}^2$. The efficiency of single-photon frequency conversion is 100% if $P_{P1} = P_{P2} = \pi^2 / (2\eta_1 L^2)$.

It is very challenging for realizing simultaneous phase matching in our work. However, this problem can be easily solved using QPM. In the experiment, we realized the broadband single photon frequency conversion of the communication band by the type-0 cascading SFG/DFG process. A 5-cm-long PPLN waveguide chip is used, and its poling period is 19.0 μm . In addition, the cascaded $\chi^{(2)} : \chi^{(2)}$ processes give rise to a large effective third nonlinearity typically $10^4 - 10^5$ times larger than a pure $\chi^{(3)}$ process, which manifests an advantage over its counterpart of FWM, e.g., in fibers.

The experimental setup of the single-photon frequency conversion is shown in **Figure 11(a)**. The center wavelengths of the two auxiliary pumps P1 and P2 are 1547.72 nm (CH37) and 1544.53 nm (CH41), respectively. Both narrow-band continuous lasers increase power through an erbium-doped fiber amplifier (EDFA). A set of DWDMs placed behind the EDFA, using 150 dB of isolation to filter out the noise generated during the EDFA amplification process. Then, we use another set of DWDMs to combine the three signals of signal single photon, P1 and P2 into one beam and couple into the waveguide. The combined light undergoes a cascaded nonlinear process SFG + DFG in the PPLN waveguide, converting the signal photons into target photons. At the output of the waveguide, we use a third set of DWDMs to pick out the target photons, while using 180 dB of isolation to filter out the noise generated during P1, P2, and conversion. In our experimental scheme, frequency-adjustable single-photon frequency conversion can be achieved by adjusting the wavelength of the auxiliary pump light.

For the performance of the converter, we tested the photon pair prepared by SPDC instead of the weak coherent pulse. The photon pair preparation process is shown in **Figure 11(b)**. After a continuous laser with a center wavelength of 1555.8 nm is amplified by EDFA power, a continuous light of 777.9 nm is generated by a frequency doubling process in a PPLN waveguide. The SPDC photon pair is prepared by pumping the second waveguide with the frequency-doubled

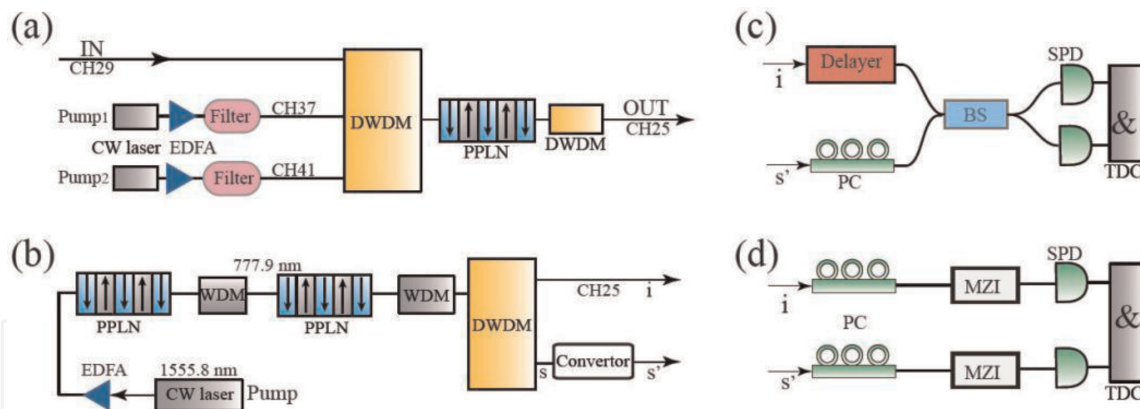


Figure 11. Experimental setup of (a) the single-photon frequency converter, (b) photon-pairs preparation, (c) Hong-Ou-Mandel interference, and (d) measurement of time-energy entanglement. DWDM, 100-GHz dense wavelength-division multiplexing; CH25 and CH37 and CH41, DWDM channels with 100-GHz spacing defined by ITU-TG.694.1; Filter, combination of DWDM and band pass filter (200–1540 and 1560–1800 nm); PC, polarization controller; SPD, single-photon detector (quantum efficiencies, $\eta_d = 10.0 \pm 0.2\%$; repetition frequency of gate, $f = 50$ MHz; width of gate, 1 ns; dark count probability per nanosecond, $D = 1 \times 10^{-6}$); EDFA, erbium-doped fiber amplifier; WDM, 780–1550-nm wavelength-division multiplexing; TDC, time-to-digital converter (coincidence time window, $t = 1$ ns); Delayer, fiber path-length delay; BS, 50:50 fiber beam splitter; MZI, 1-GHz unbalanced planar lightwave circuit Mach-Zehnder interferometers [7].

continuous light. WDM with an isolation of 180 dB is used to filter out noise. Finally, the corresponding two channels in signal (1554.13 nm, CH29) and idler (1557.36 nm, CH25) DWDM are separated.

First, we use classical light to test the conversion efficiency of tunable frequency conversion. By changing the center wavelength of the auxiliary pump P2, we achieved frequency conversion of the signal photon ± 12 DWDM channels. In the classic light test, we set the signal power to 1 mW, and both P1 and P2 have a power of 10 mW (because the PPLN waveguide is limited by thermal effects, the maximum total input power of the waveguide we use for conversion is around 20 mW). We can get that the theoretical value is in good agreement with the experimental value, and the conversion efficiency of ± 12 CH is about 0.8%. In theory, the tunable frequency conversion has a full width at half maximum of about 76 nm, which covers the entire communication C-band.

In our experiment, the photon-pair generation rate is set to 0.002 per detection gate. The maximum single-photon conversion efficiency in the experiment is that when $P_{P1} = P_{P2} = 10$ mW, the maximum number of converted photons is 5.5×10^4 /s, and the conversion efficiency is calculated to be 0.55%. At the same time, we measured that the noise generated by the frequency conversion process is 10^{-7} /gate. When the incident power of both auxiliary pumps is 179.5 mW, 100% conversion efficiency can be obtained. However, there are three main reasons for the reduction in conversion efficiency in actual experiments. The first reason is that the thermal effect of the PPLN waveguide limits the power of the incident light. This limitation is also the most important cause of the drop in conversion efficiency. We know that if a PPLN waveguide doped with MgO is used, the damage threshold can be greatly improved without changing the scattering properties of its refractive index, and it can withstand the total incident power of 360 mW. Another reason is the phase difference between the two auxiliary pumps P1 and P2, and we get the conversion efficiency proportional to $|\varphi_1 - \varphi_2|$. Since there is no synchronous lock between the phase differences between P1 and P2 in our experiments, $|\varphi_1 - \varphi_2|$ is equal to 0.5 after averaging over time. This reason will directly lead to a 50% reduction in conversion efficiency. The last reason is also the problem that

other frequency conversion methods will encounter, namely, the loss of fiber coupling and the loss caused by the filter. In our experiment, the total propagation and coupling loss in the PPLN waveguide and the filters is only 4.9 dB.

After measuring the maximum conversion efficiency experimentally, we measured the conversion accuracy of our single-photon frequency converter by HOM interference. The experimental setup for HOM interference is shown in **Figure 11(c)** [14], where i' is the idler photon in the photon pair and s' represents the converted signal photon. We placed a fiber optic delay in the i -photon beam path (Delay, Delayer has an adjustment accuracy of 0.02 mm.), Delayer is used to change the optical path difference δx between i and s' ; placing polarization control in the s' photon path (PC), PC is used to change the polarization of the s' photon to match the polarization of the i -photon, because the HOM interference visibility of the identical particles is best. In our experiments, the ratio of BS transmittance to reflectance used in our experiments was measured as T:R = 49.9:50.1. The single-photon detector used in this experiment is still a pulse gate detection method, but the performance is upgraded. The dark counts of both detectors are $D = 1 \times 10^{-6}$ per gate.

In HOM, we set the photon pair generation rate $\mu = 0.002$ per gate; the single photon conversion efficiency is set to the maximum conversion efficiency under the constraint condition, i.e., 0.55%; and the measurement time of each data point is 1000 s. Under these conditions, the HOM interference curve we measured is shown in **Figure 12**. The calculated HOM interference visibility of the converted photon pair is $(80.5 \pm 3.5)\%$, and this contrast is much larger than the classical and non-classical limit of 50%, which proves that our single photon converter does. We further analyzed the HOM interference gram and found that the full width at half maximum of the interference gram is 0.56 mm, and the corresponding time is 0.28 ps. Our theoretical full width at half maximum is about 0.50 mm; thus, the theoretical and experimental results are more consistent.

In addition to the true conversion of this feature, another important feature of single-photon frequency conversion is the preservation of quantum properties. As with some previous quantum frequency converters, we demonstrate that the quantum properties are not corrupted during the conversion process by measuring the quantum state visibility of the photon pairs before and after the conversion. In our experiments, the signal and idler photon pairs were prepared as time-energy entangled photon pairs. The time-energy entanglement pair is generated by a

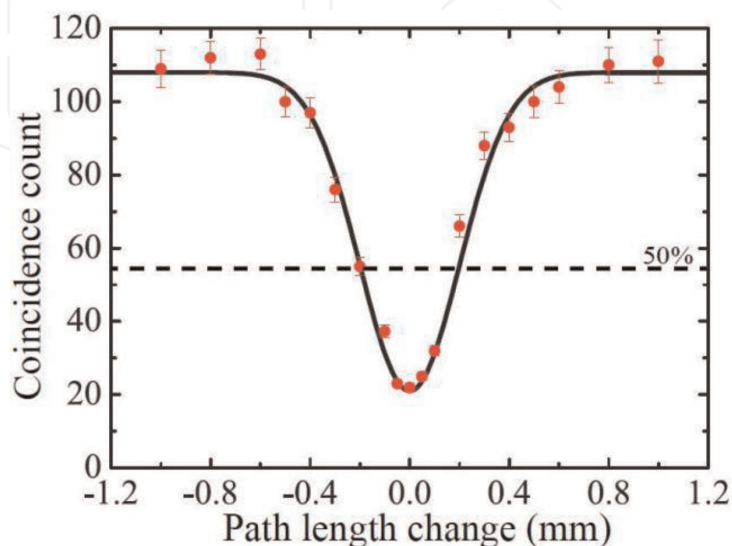


Figure 12.

Coincidence count as a function of the path-length change of one photon. The standard deviation is calculated by assuming a Poisson distribution of photon counts. The dashed horizontal line at 50% is the dividing line between the classical and nonclassical interference [7].

continuous laser (cw-laser) pumping the PPLN waveguide through the SPDC process [15]. Because the coherence time τ_1 of cw-laser is extremely long, and the bandwidth of the down-converted photon pair is much larger than the bandwidth of the pump photon, that is, the coherence time τ_2 between photon pairs is very short.

To measure the characteristics of time-energy entanglement and to exploit this entanglement, we use two unbalanced Mach-Zehnder interferometers (MZI) as shown in **Figure 11(d)**, connecting a single photon detector at the output of the MZI, measuring two coincidence count at the output. We define the optical path difference of the two paths of the MZI interferometer as τ_3 . It is assumed that when $\tau_1 \geq \tau_3 > \tau_2$, the exit end of MZI does not have a single photon interference image, and the image of two-photon interference can be observed by the coincidence measurement.

The MZI used in our experiments is to change the phase difference between the long and short arms by adjusting the temperature. The phase change of 2π corresponds to a temperature change of 0.7° . The entangled interference image before single-photon frequency conversion is shown in **Figure 13**. Because it is necessary to observe the interference image under the two non-collinear base vectors, we can prove that the two-photon is entangled, so we set the MZI temperature of the signal

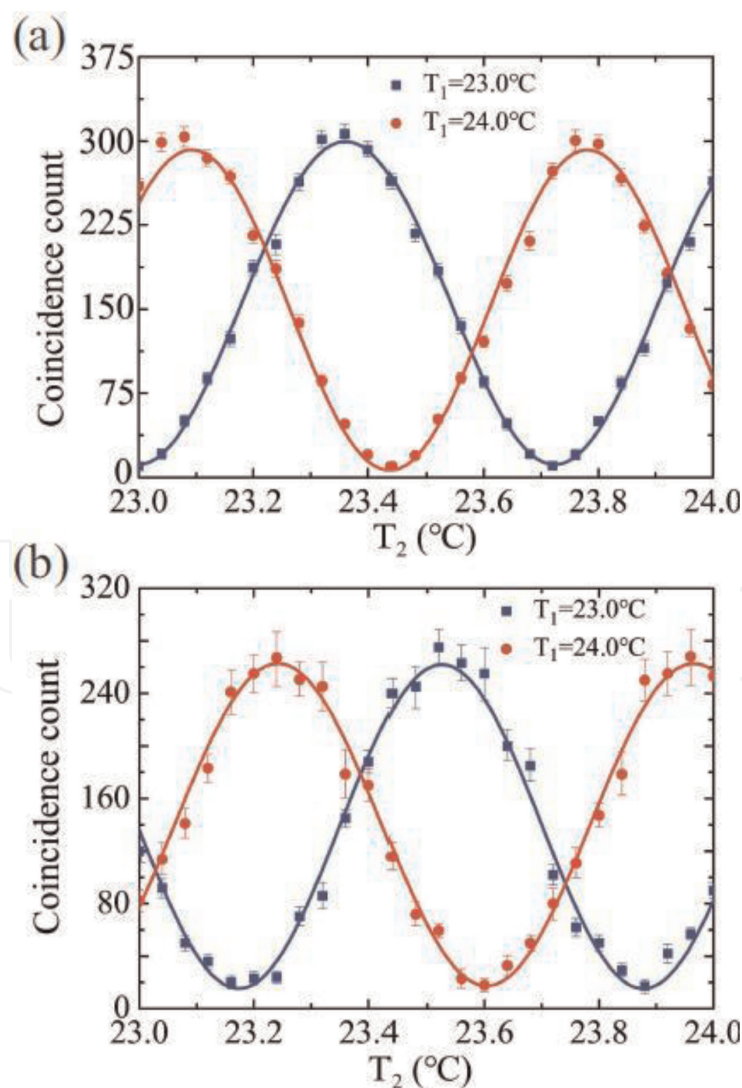


Figure 13. Two-photon interference pattern (a) before and (b) after the frequency conversion. T_1 is the temperature of the MZI in the signal channel, and T_2 is the temperature in the idler channel. The integration time for each dot is (a) 15 s and (b) 3000 s [7].

channel to 23.0 and 24.0°, respectively. The collinear base vector is measured. From **Figure 13(a)**, we calculated the average pre-conversion entanglement visibility as $V = (93.8 \pm 1.6)\%$.

After the single photon frequency conversion, we again measure the entanglement visibility of the converted photon pair, as shown in **Figure 13(b)**. It is calculated that the converted entanglement visibility is $V = (88.2 \pm 5.1)\%$, and this visibility can still break the 71% visibility of Bell's inequality. Therefore, the 88.2% visibility after conversion proves that our single-photon frequency converter maintains the quantum properties of photons with a theoretical visibility of 91%. Since the converted count efficiency is low, the measurement time is extended from 15 s before conversion to 1000 s. The result convincingly shows that quantum entanglement is well preserved during the frequency conversion. Thus, the photon pairs can still be used for quantum communication tasks. We expect that our scheme may have applications in quantum systems, such as quantum communication on multiuser fiber quantum networks and quantum cryptography with independent single photon sources.

3. Conclusion

We have demonstrated three kinds of quantum interfaces with different functions. First, we have experimentally demonstrated that the spectrum of single-photon-level laser pulse was compressed by a factor of 58 in a PPLN waveguide chip, where a chirped single-photon-level laser pulse and an antichirped laser pulse by fiber Bragg gratings are used to achieve a pulse with new frequency through SFG. Our results have demonstrated the potentially application for PPLN waveguide chip as an integrated platform for spectrum compressing and frequency conversing in the telecom band, such as coherent photonic interfaces between quantum communication at 1550 nm and quantum memory in the near-visible window. Second, we have realized high efficiency SFG between two broadband single-photon-level coherent states by using a high-efficiency PPLN waveguide chip. The result is already competitive with methods based on linear optics, and offers new possibilities such as heralding entanglement at a distance. This technique in our proposal marks a critical step toward the implementation of DI-QKD. Final, we have demonstrated single-photon frequency conversion using a cascaded quadratic nonlinearity in PPLN waveguides chip. The clear HOM dip observed in our experiment shows that the frequency has been precisely switched between DWDM channels. Moreover, the time-energy entanglement is well preserved during the frequency conversion. All works above are of great significance to the development of quantum optics.

Conflict of interest

The authors declare no conflict of interest.

IntechOpen

Author details


Yuanhua Li^{1*} and Xianfeng Chen²

¹ Department of Physics, Jiangxi Normal University, Nanchang, China

² State Key Laboratory of Advanced Optical Communication Systems and Networks, Department of Physics and Astronomy, Shanghai Jiao Tong University, Shanghai, China

*Address all correspondence to: lyhua1984@163.com

IntechOpen

© 2019 The Author(s). Licensee IntechOpen. This chapter is distributed under the terms of the Creative Commons Attribution License (<http://creativecommons.org/licenses/by/3.0>), which permits unrestricted use, distribution, and reproduction in any medium, provided the original work is properly cited. 

References

- [1] Sun QC, Mao YL, Chen SJ, Zhang W, Jiang YF, Zhang YB, et al. Quantum teleportation with independent sources and prior entanglement distribution over a network. *Nature Photonics*. 2016; **10**(10):671-675. DOI: 10.1038/nphoton.2016.179
- [2] Miller J, Miyake A. Resource quality of a symmetry-protected topologically ordered phase for quantum computation. *Physical Review Letters*. 2015; **114**(12):120506. DOI: 10.1103/PhysRevLett.114.120506
- [3] Specht HP, Nölleke C, Reiserer A, Uphoff M, Figueroa E, Ritter S, et al. A single-atom quantum memory. *Nature*. 2011; **473**(7346):190-193. DOI: 10.1038/nature09997
- [4] Yurke B, Denker JS. Quantum network theory. *Physical Review A*. 1984; **29**(3):1419. DOI: 10.1103/PhysRevA.29.1419
- [5] Li YH, Xiang T, Nie YY, Sang MH, Chen XF. Spectral compression of single-photon-level laser pulse. *Scientific Reports*. 2017; **7**:43494. DOI: 10.1038/srep43494
- [6] Li YH, Xiang T, Nie YY, Sang MH, Chen XF. Nonlinear interaction between broadband single-photon-level coherent states. *Photonics Research*. 2017; **5**(4): 324-328. DOI: 10.1364/PRJ.5.000324
- [7] Xiang T, Sun QC, Li YH, Zheng YL, Chen XF. Single-photon frequency conversion via cascaded quadratic nonlinear processes. *Physical Review A*. 2018; **97**(6):063810. DOI: 10.1103/PhysRevA.97.063810
- [8] Lavoie J, Donohue JM, Wright LG, Fedrizzi A, Resch KJ. Spectral compression of single photons. *Nature Photonics*. 2013; **7**(5):363-366. DOI: 10.1038/nphoton.2013.47
- [9] Thew RT, Zbinden H, Gisin N. Tunable upconversion photon detector. *Applied Physics Letters*. 2008; **93**(7): 071104. DOI: 10.1063/1.2969067
- [10] Shalm LK, Hamel DR, Yan Z, Simon C, Resch KJ, Jennewein T. Three-photon energy-time entanglement. *Nature Physics*. 2013; **9**(1):19-22. DOI: 10.1038/nphys2492
- [11] Matsuda N, Shimizu R, Mitsumori Y, Kosaka H, Edamatsu K. Observation of optical-fibre Kerr nonlinearity at the single-photon level. *Nature Photonics*. 2009; **3**(2):95-98. DOI: 10.1038/nphoton.2008.292
- [12] Sangouard N, Sanguinetti B, Curtz N, Gisin N, Thew R, Zbinden H. Faithful entanglement swapping based on sum-frequency generation. *Physical Review Letters*. 2011; **106**(12):120403. DOI: 10.1103/PhysRevLett.106.120403
- [13] Kumar P. Quantum frequency conversion. *Optics Letters*. 1990; **15**(24): 1476-1478. DOI: 10.1364/OL.15.001476
- [14] Hong CK, Ou ZY, Mandel L. Measurement of subpicosecond time intervals between two photons by interference. *Physical Review Letters*. 1987; **59**(18):2044-2046. DOI: 10.1103/PhysRevLett.59.2044
- [15] Franson JD. Bell inequality for position and time. *Physical Review Letters*. 1989; **62**(19):2205-2208. DOI: 10.1103/PhysRevLett.62.2205